ACS APPLIED ENERGY MATERIALS

www.acsaem.org Article

Engineering Cu_2O Nanowire Surfaces for Photoelectrochemical Hydrogen Evolution Reaction

Getachew Solomon, Marco Lecca, Matteo Bisetto, Mojtaba Gilzad Kohan, Isabella Concina, Marta Maria Natile,* and Alberto Vomiero*

Cite This: *ACS Appl. Energy Mater.* 2023, 6, 832−840 Read Online

ACCESS | Metrics & More | Article Recommendations | Supporting Information

ABSTRACT: Cu_2O is a narrow band gap material serving as an important candidate for photoelectrochemical hydrogen evolution reaction. However, the main challenge that hinders its practical exploitation is its poor photostability, due to its oxidation into CuO by photoexcited holes. Here, we thoroughly minimize the photo-oxidation of Cu_2O nanowires by growing a thin layer of the TiO_2 protective layer and an amorphous layer of the VO_x cocatalyst using magnetron sputtering and atomic layer deposition, respectively. After optimization of the protective and the cocatalyst layers, the photoelectrode exhibits a current density of −2.46 mA/cm^2 under simulated sunlight (100 mW/cm^2) at 0.3 V versus reversible hydrogen electrode, and its performance is stable for an extended illumination time. The chemical stability and the good performance of the engineered photoelectrode demonstrate the potential of using earth-abundant materials as a light-harvesting device for solar hydrogen production.

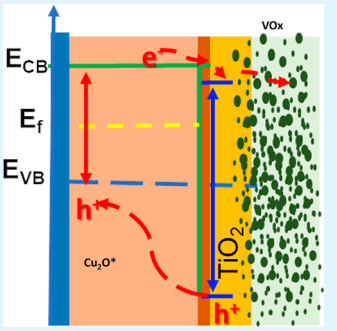

KEYWORDS: *photoelectrochemical hydrogen evolution, Cu_2O photoelectrode, atomic layer deposition, magnetron deposition, water splitting*

1. INTRODUCTION

Photoelectrochemical (PEC) water splitting is a process that uses solar energy absorbed by a semiconductor to convert water into molecular hydrogen and oxygen. Apart from its very low efficiency, the mechanism is one of the promising pathways for sustaining renewable hydrogen production. PEC devices use light-absorbing semiconductors that can absorb solar energy and perform water electrolysis.[1−3] It is challenging to obtain semiconductors that act as a catalyst for hydrogen evolution reaction (HER) and absorb light at the same time. In addition, both the water-splitting process and the light absorption have issues to be solved. In most cases, the light energy absorbed by the photocathode is insufficient to drive water electrolysis. Due to this reason, different strategies, such as the use of heterostructures, the addition of a cocatalyst, and doping, have been employed for absorbing a larger portion of visible light and for improving the catalysis process on the surface of the photocathode.[4−7] The photons with energy equal to or greater than the energy gap of the semiconductor can excite an electron from the valence band to the conduction band, generating electrons in the conduction band and holes in the valence band. At the photocathode, the electrons generated by the photons reach the surface of the electrode and participate in the HER process, while the photogenerated holes on the semiconductor surface unleash oxidation reactions.[4,5]

Copper(I) oxide has been employed as a semiconductor for PEC water splitting, due to its availability, low toxicity, and favorable band positions.[8] In addition, Cu_2O is a p-type semiconductor with a band gap of around 2 eV capable of absorbing visible light. More interestingly, the conduction band position is suitable for light-driven HER.[8−10] Even though it has many interesting electronic properties, Cu_2O also shows some drawbacks that hinder its application as a photoactive material. The poor stability in aqueous solution is one of the main problems, which is due to the ease of oxidation of copper(I).

In this work, a heterostructure based on Cu_2O nanowires is employed as a photocathode for PEC hydrogen evolution, and the abovementioned limitation is systematically minimized through different approaches. In several investigations, the TiO_2 film, mostly deposited by atomic layer deposition (ALD), was considered as a protective layer to avoid the photo-oxidation of Cu_2O.[9,11−14] However, the oxidizing agent (water or ozone) commonly used to oxidize the titanium precursors can also favor in situ oxidation of the Cu_2O nanowires before they are covered by the protective layer. To overcome this problem, we use magnetron sputtering to deposit a thin layer of TiO_2 under ultra-high vacuum conditions. This technique, in fact, provides a controlled, scalable, and repeatable deposition without affecting the bare materials.[15,16] Next,

Received: September 23, 2022
Accepted: December 15, 2022
Published: January 2, 2023

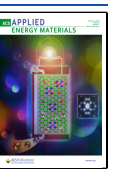

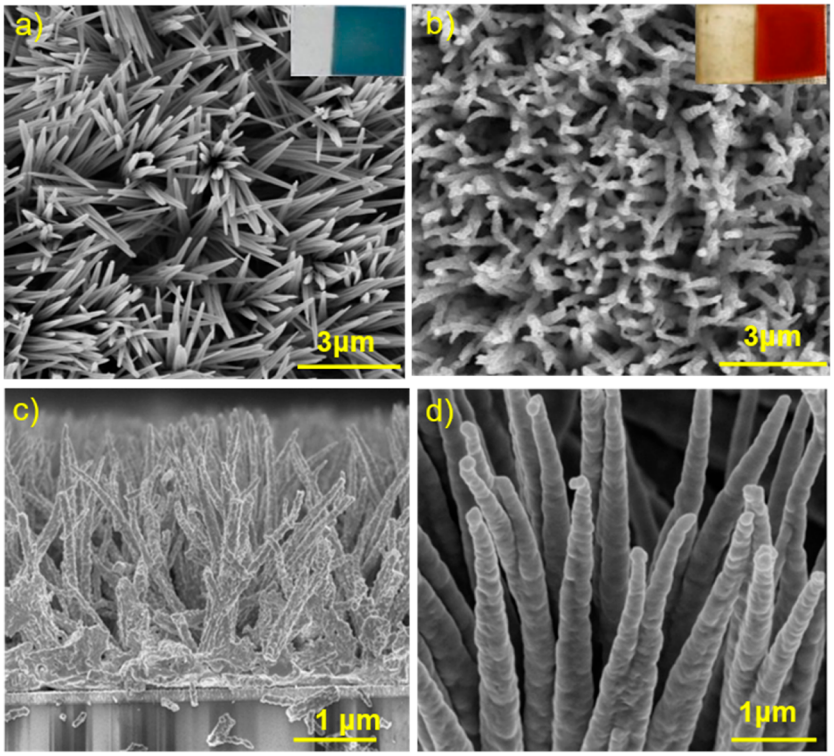

Figure 1. SEM images of (a) $Cu(OH)_2$ nanowires. (b) Cu_2O nanowire after annealing. Insets in (a,b) are photographs of the FTO substrate coated with $Cu(OH)_2$ and Cu_2O nanowires, respectively. (c) Cu_2O nanowire cross-sectional view and (d) Cu_2O/TiO_2 with 700 ALD cycles of VO_x.

ALD is applied to conformally cover the Cu_2O/TiO_2 composite electrode with an amorphous VO_x thin film. The presence of the n-type TiO_2 semiconductor forms a p−n junction and acts as a protective layer for Cu_2O. The VO_x layer increases the surface-active site densities and acts as a cocatalyst in the PEC HER performance.

2. MATERIALS AND METHODS

2.1. Photoelectrode Preparation. *2.1.1. Copper Film Deposition.* A pure copper film was deposited on FTO glass substrates (TEC 15 from Pilkington) by magnetron sputtering (Minilab 060 from Moorfield Nanotechnology) using a copper (99.99%) target (from Kurt J Lesker Company Ltd). Optimized deposition conditions such as an operating pressure of 1.4×10^{-3} mbar and a substrate temperature of 100 °C were used to improve adhesion. The deposition was conducted in argon gas flow (20 sccm). A film with a thickness of 1.8 μm was obtained after 45 min deposition.

2.1.2. Cu_2O Nanowires Synthesis. First, the $Cu(OH)_2$ nanowires were prepared by galvanostatic anodization of the as-deposited Cu film on the FTO substrate by adapting a previous procedure.[9] A potentiostat (Modulab XM ECS of Solartron Analytical) with a two-electrode configuration was used. The copper-coated FTO substrate and graphite electrodes were used as working and counter electrodes, respectively. Briefly, a current density of 10 mA/cm^2 was applied for 180 s at room temperature (RT) in a 3.0 M KOH (Merk) solution. Before anodization, the solution was kept under argon gas flow for 15 min. After anodization, the electrode was carefully washed with deionized water and then dried in air. The conversion of $Cu(OH)_2$ into Cu_2O nanowires was performed by a heat treatment at 500 °C under an argon atmosphere for 4 h.

2.1.3. TiO_2 Protective Layer Deposition. A 10 nm TiO_2 layer was deposited by reactive magnetron sputtering from a titanium target (purity 99.99%) and a 95% Ar + 5% O_2 atmosphere. The deposition was made at RT, at a pressure of 1.4×10^{-3} mbar. The time to obtain a film thickness of 10 nm was 90 s with an average growth rate of 4.44 Å/s referred to as a smooth surface. In addition, 20 and 40 nm TiO_2 layers were tested for optimization purposes.

2.1.4. VO_x Layer Synthesis. The film was deposited using Savannah 200 of the Cambridge Nanotech ALD system. Vanadium (V) oxytriisopropoxide [VTIP, (Sigma-Aldrich)] and distilled water were used as metal and oxidizing agents, respectively. The VTIP precursor was preheated at a temperature of 75 °C. The deposition was conducted at 150 °C, with a pulse time of 0.15 s for the vanadium precursor and 0.03 s for water, while the purge time was in both cases 20 s. Pure nitrogen was used as a gas carrier. Keeping the rate of growth constant at 0.51 Å/cycle and by simply adjusting the number of deposition cycles, amorphous films of 500 ALD cycles, 700 ALD cycles, and 1000 ALD cycles were grown on top of the Cu_2O/TiO_2 heterojunction. We labeled the cocatalyst as VO_x to show its amorphous nature.

2.1.5. Cu_2O Layer Synthesis. An additional layer of Cu_2O was electrodeposited on the bare Cu_2O nanowires obtained after the heat treatment at 500 °C. A potentiostat Modulab XM ECS of Solartron Analytical was used in a three-electrode configuration with the bare FTO/Cu_2O electrode, a Pt foil, and a saturated calomel electrode (SCE) as working, counter, and reference electrode, respectively. A 15 mL solution obtained by mixing 4 mL of 11.3 M lactic acid (Sigma-Aldrich) and 11 mL of 0.5 M solutions of $CuSO_4 \cdot 5H_2O$ (Merk) was used as the electrolyte. The pH was adjusted to 9.2 by adding KOH (Merk). Before starting with electrodeposition, the electrolyte was left under magnetic stirring and an argon atmosphere for 20 min to evacuate molecular oxygen and to avoid the oxidation of the electrode. The electrochemical deposition of Cu_2O was carried out at 80 °C for 300 s in an argon atmosphere, setting up the potentiostatic mode with −0.35 V versus SCE.

2.2. Characterization. *2.2.1. Material Characterization.* The morphology of the as-synthesized photoelectrodes was investigated using field emission scanning electron microscopy (SEM) equipped with an Oxford INCA X-sight detector for energy dispersive X-ray spectroscopic (EDS) analyses. The X-ray diffraction (XRD) analysis of photoelectrodes was carried out using a PANalytical Empyrean X-ray diffraction diffractometer with a Cu Kα source. Raman spectra

https://doi.org/10.1021/acsaem.2c03122
ACS Appl. Energy Mater. 2023, 6, 832−840

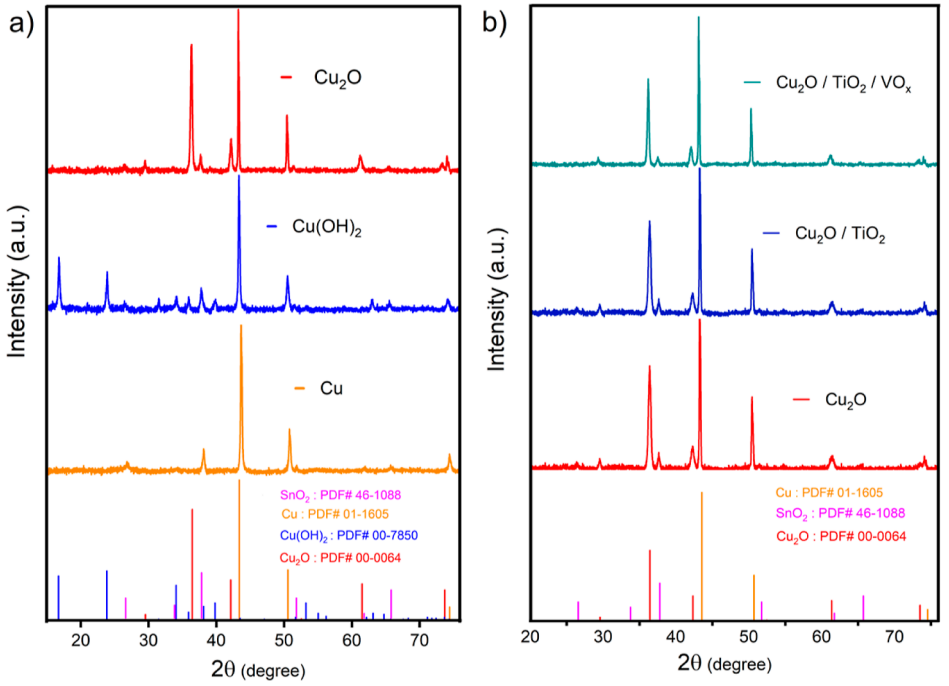

Figure 2. XRD patterns of the photoelectrode after each step of preparation: (a) Cu, $Cu(OH)_2$, and Cu_2O and (b) Cu_2O, Cu_2O/TiO_2, and $Cu_2O/TiO_2/VO_x$ (700 ALD cycles of VO_x). On the bottom, the XRD reference patterns from the PDF card are reported for comparison.

were collected using a Senterra Raman spectrometer (Bruker) equipped with a 532 nm laser for excitation in the ambient environment with 2 mW laser power. Ultraviolet−visible absorption spectra were recorded on a Cary 5000 spectrometer (Agilent). Rutherford backscattering spectrometry (RBS) was applied for compositional and thickness measurement, using a 1.8 MeV $^4He^+$ beam in IBM geometry and with scattering angle θ = 160°. The measurement was conducted on TiO_2 samples deposited on a silicon substrate. RUMP code simulation was utilized for calculating the atomic ratio and film thickness.

2.2.2. Photoelectrochemical Characterization. PEC properties toward HER were analyzed using the Modulab XM ECS potentiostat from Solartron Analytical, using a three-electrode configuration at RT. An SCE and a Pt plate were used as the reference and counter electrodes, respectively. A solution containing 0.5 M Na_2SO_4 (Riedel-de Haen) and 0.1 M K_2HPO_4 (Sigma-Aldrich) was used as the electrolyte. The reported potential was calibrated to a reversible hydrogen electrode (RHE), using the formula E (vs RHE) = E (vs SCE) + 0.059 × pH + 0.242 V. Electrochemical impedance spectroscopy (EIS) was carried out in the range of frequencies from 100 kHz to 3 mHz at −0.25 V versus RHE by applying 10 mV AC perturbation. A light source (SOLIS-1D-High-Power LED, with a power output of 100 mW cm^{-2}) was used for photocurrent measurement.

3. RESULTS AND DISCUSSION

3.1. Engineering Cu_2O Nanowire Surfaces. $Cu(OH)_2$ nanowires were successfully synthesized by anodizing the smooth 1.8 μm Cu thin film (Figure S1a in the Supporting Information) deposited by magnetron sputtering on the FTO glass substrate (see the Materials and Methods section for more detail on the conditions used for magnetron sputtering). Grätzel et al.[9] showed by several experiments that an excess of metal copper from the substrate was necessary to convert $Cu(OH)_2$ nanowires prepared by galvanostatic anodization into Cu_2O nanowires. In particular, they demonstrated that a Cu film with a thickness >1.5 μm was mandatory to obtain pure Cu_2O nanowires, while for a lower thickness, a mixture of Cu_2O and CuO (Cu thickness 0.5−1.5 μm) or pure CuO (Cu thickness <0.5 μm) was formed. With this result in mind, we decided to use the 1.8 μm Cu thin film on FTO to grow $Cu(OH)_2$ nanowires.

The thermal treatment of Cu $(OH)_2$ nanowires under an argon atmosphere led to dehydration and formation of Cu_2O, preserving the nanowire shape, but an increase in the roughness of the nanowire surface was observed (Figures 1b and S1b). As a matter of fact, the single-crystal Cu $(OH)_2$ nanowires were converted into Cu_2O polycrystalline nanowires (Figure 1b). The successful conversion of $Cu(OH)_2$ into Cu_2O was also confirmed by a change in color: the light blue color typical of $Cu(OH)_2$ is replaced by a reddish color typical of Cu_2O after annealing (see insets in Figure 1a,b). The cross-sectional SEM analysis of Cu_2O nanowires (Figure 1c) evidenced that the length of nanowires is in the range of 100−400 nm. A thin layer of TiO_2 acting like a protective layer was deposited by magnetron sputtering on the annealed Cu_2O nanowires (Figure 1d).

The morphology of the Cu_2O nanowires is not visibly affected by the deposition of the TiO_2 layer and by the subsequent deposition of the VO_x cocatalyst by ALD (Figure 1d). EDS mapping (Figures S2−S4) shows a homogeneous distribution of the expected species after each step. For bare Cu_2O nanowires, the EDS quantitative analysis reveals a Cu/O ratio of 2.6:1 compatible with the presence of Cu_2O. The EDS map sum shows the presence of both Ti and V, suggesting the presence of the TiO_2 protective layer and VO_x cocatalyst on the surface of the nanowires (Figures S3 and S4 in the Supporting Information).

In Figure 2a,b, the XRD patterns of the Cu_2O photocathode after each step of preparation are provided. The analysis of the XRD pattern collected after the deposition of the Cu thin film by magnetron sputtering reveals the typical reflections of polycrystalline metallic Cu (PDF# 01-1605), besides small reflections characteristic of the SnO_2 from the FTO glass

https://doi.org/10.1021/acsaem.2c03122
ACS Appl. Energy Mater. 2023, 6, 832−840

substrate (PDF# 46-1088). After anodization, new reflections characteristic of $Cu(OH)_2$ with a spertiniite phase (PDF# 00-7850) appear, which then give way to reflections of Cu_2O (PDF# 00-0064) after the thermal treatment.[17−19] The contributions from FTO and, in particular, metallic Cu are still evident after the anodization and thermal treatment, confirming that not all the Cu substrate is oxidized. The XRD patterns collected on the photocathode after the deposition of the TiO_2 protective layer (Cu_2O/TiO_2) and VO_x cocatalyst ($Cu_2O/TiO_2/VO_x$) are quite similar to that of the Cu_2O system: no reflections characteristic of crystalline TiO_2 and VO_x are visible, suggesting their amorphous nature (Figure 2b). The slight progressive decrease in the relative intensity of Cu_2O contributions with respect to metallic ones moving from Cu_2O to $Cu_2O/TiO_2/VO_x$ confirms the nanowire coating.

The analysis of Raman spectra of the $Cu(OH)_2$, Cu_2O, Cu_2O/TiO_2, and $Cu_2O/TiO_2/VO_x$ cathodes provided additional information on the structural properties (Figure 3).

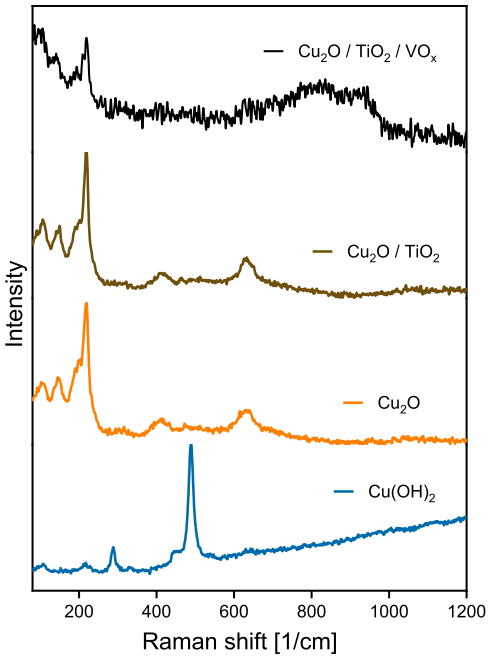

Figure 3. Raman spectra of $Cu(OH)_2$, Cu_2O, Cu_2O/TiO_2, and $Cu_2O/TiO_2/VO_x$ (700 ALD cycles VO_x).

$Cu(OH)_2$ nanowires display two Raman peaks at 284 and 487 cm^{-1} characteristic of $Cu(OH)_2$ in agreement with the literature.[8,17−19] After the heat treatment, the bare Cu_2O electrode displays peaks in the region from 50 to 700 cm^{-1} (at 106, 146, 218, and 628 cm^{-1}), which are characteristic of cuprous oxide.[18] The Raman spectrum collected after deposition of TiO_2 on Cu_2O nanowires (Cu_2O/TiO_2) is very similar to that of the bare Cu_2O electrode: it does not show any new Raman-active species. The deposition of 700 ALD cycles of VO_x decreases the Raman intensities of Raman peaks attributed to Cu_2O due to the increased thickness of the amorphous layers. Moreover, a broad Raman peak between 800 and 970 cm^{-1} characteristic of amorphous VO_x[20−22] confirms the presence of the cocatalyst.

3.2. Photoelectrochemical Characterization.

3.2.1. $Cu_2O/TiO_2/VO_x$ Photocathode. The PEC properties of the photoelectrode were studied using three-electrode configuration, as described in the experimental part. Linear sweep voltammetry (LSV) was carried out on the bare Cu_2O, Cu_2O/TiO_2, and $Cu_2O/TiO_2/VO_x$ electrode (Figure 4a−d). Under dark conditions, the bare Cu_2O electrode shows a very low current density, around −0.06 mA/cm^2 at −0.2 V versus RHE. Under light illumination, the current density increases to −0.96 mA/cm^2, showing the characteristic photoactive nature of Cu_2O. After a repeated LSV scan, the performance of bare Cu_2O decreases as shown in the LSV curve (Figure 4a, labeled light*), confirming its poor photostability. After deposition of the TiO_2 protective layer, the photoelectrode displays a similar phenomenon (Figure 4b): the repeated scan under light conditions (light*) shows a decrease with time, suggesting that the photo-oxidation of bare Cu_2O is still occurring.

The LSV of the Cu_2O/VO_x layer displayed low photocurrent (Figure 4c), evidenced by the overlap of the LSV under dark and light illumination. This behavior highlights the importance of introducing a TiO_2 between Cu_2O and VO_x. After the deposition of VO_x on the surface of the Cu_2O/TiO_2 cathode, an increase in the photocurrent is evident both under dark and light illumination conditions (Figure 4d). Under light illumination, the electrode covered with VO_x results in a photocurrent of −2.37 mA/cm^2 at −0.2 V versus RHE, while the dark current at the same potential is −0.59 mA/cm^2. These results point out that the enhanced PEC performance of the $Cu_2O/TiO_2/VO_x$ photoelectrode can be ascribed to both the TiO_2 layer, effectively protecting the Cu_2O from oxidation, and the VO_x cocatalyst, increasing the number of charge carriers reaching the electrode surface. However, after a consecutive LSV scan, a small decrease in the photoresponse is evident, similar to the other photoelectrodes.

The decrease in photocurrent over time, even with the presence of the TiO_2 protective layer and the VO_x cocatalyst, could be due to the direct contact between the TiO_2 and the Cu metal film not fully anodized. This creates low resistance charge flows and increases the recombination rate as reported in a recent work.[9]

3.2.2. Optimization of the Photocathode: $Cu_2O^*/TiO_2/VO_x$. To minimize the problems due to the direct contact of the TiO_2 protective layer with the Cu substrate and to improve the performance of the Cu_2O-based photoelectrode, we decided to better isolate the metallic copper substrate by adding a further layer of Cu_2O on the nanowires before the deposition of the TiO_2 film. Therefore, an additional layer of Cu_2O was electrodeposited on the bare Cu_2O nanowires (the bare Cu_2O nanowires together with the additional electrodeposited Cu_2O layer are labeled Cu_2O^* hereafter). This additional layer should homogeneously cover both the nanowires and the metallic Cu, which is not affected by the anodization process, and avoid the formation of the Schottky contact. Figure 5a,b shows the SEM image of the $Cu_2O^*/TiO_2/VO_x$ (700 ALD cycles) heterostructure. As expected, the electrodeposited Cu_2O layer contributes to increase the width of the nanowires compared to bare Cu_2O nanowires (Figure 1b). Thickness and stoichiometry of TiO_2 films deposited on Cu_2O were determined by RBS analysis on a TiO_2 sample deposited under the same conditions on the silicon substrate (Figure S5a). The presence of O and Ti was confirmed by the increase in the yield of the high-energy signal in channels 520 and 840, respectively. The RBS spectra display both the experimental and simulated data of the TiO_2/silicon sample using the Rump simulation. The film thickness is 10 nm, and the composition ratio of Ti/O is obtained to be 1:2. The Raman spectra and XRD patterns of the Cu_2O-based

https://doi.org/10.1021/acsaem.2c03122
ACS Appl. Energy Mater. 2023, 6, 832−840

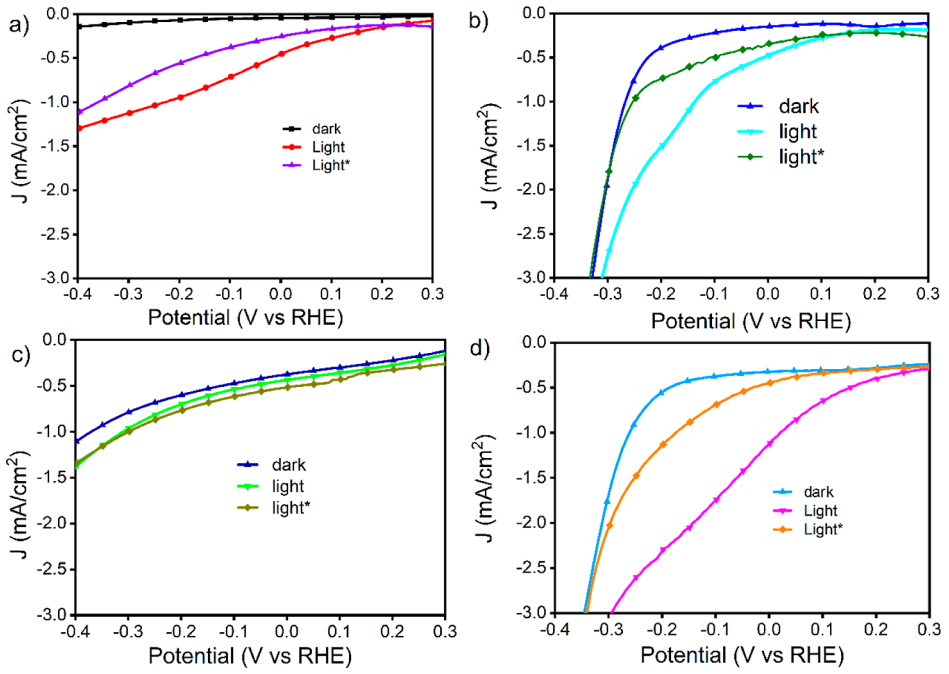

Figure 4. LSV of (a) bare Cu_2O, (b) Cu_2O/TiO_2, (c) Cu_2O/VO_x, and (d) $Cu_2O/TiO_2/VO_x$ (700 ALD cycles) under dark and light illumination conditions. The LSV labeled light* denotes the measurements of the photocathode recorded after five repeated LSV scans for comparing the photostability.

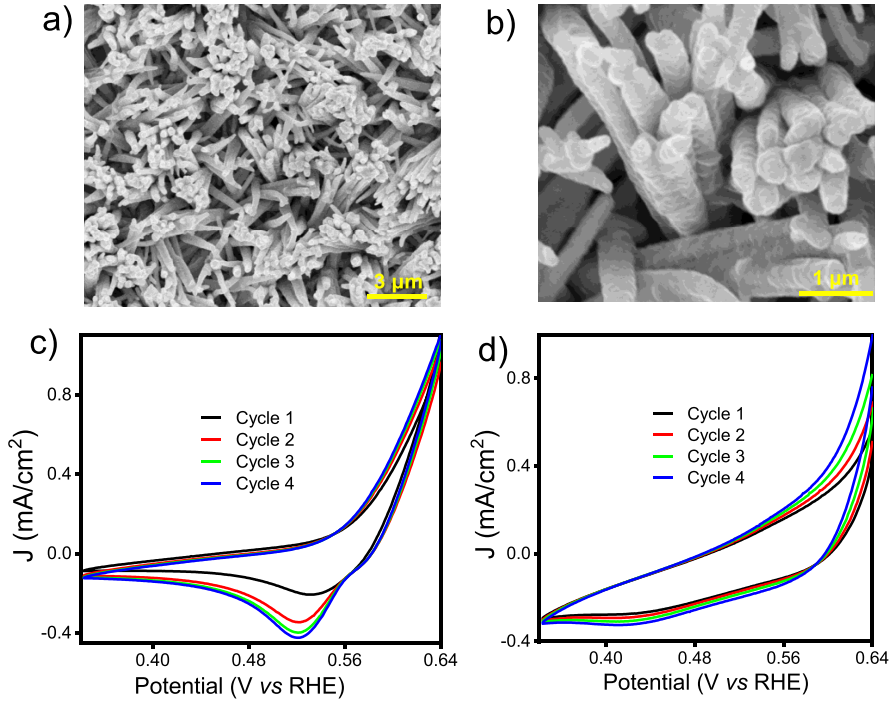

Figure 5. (a,b) SEM images of $Cu_2O^*/TiO_2/VO_x$ (700 ALD cycles) and (c,d) CVs of bare Cu_2O and $Cu_2O^*/TiO_2/VO_x$ (700 ALD cycles), respectively.

photoelectrodes with the electrodeposited Cu_2O layer (Cu_2O^*) are similar to those of the bare Cu_2O nanowires: no other phases form during the electrodeposition process [see Supporting Information, Figures S5b (Raman), S6 (XRD), and S7 (EDS)]. In Figure S7, the EDS maps of the new $Cu_2O^*/TiO_2/VO_x$ photoelectrode also displays the presence of all the expected elements.

To assess the effectiveness of the coating layers in preventing the Cu_2O oxidation, cyclic voltammograms (CVs) were collected for both the bare Cu_2O and $Cu_2O^*/TiO_2/VO_x$ photoelectrodes (Figure 5c,d). Bare Cu_2O nanowires display a reduction peak around 0.52 V versus RHE (Cu^+ reduction), associated with the surface-oxidized form of Cu_2O.[23,24] However, such a reduction peak is not observed when the electrodeposited Cu_2O, TiO_2 protective layer, and the

https://doi.org/10.1021/acsaem.2c03122
ACS Appl. Energy Mater. 2023, 6, 832−840

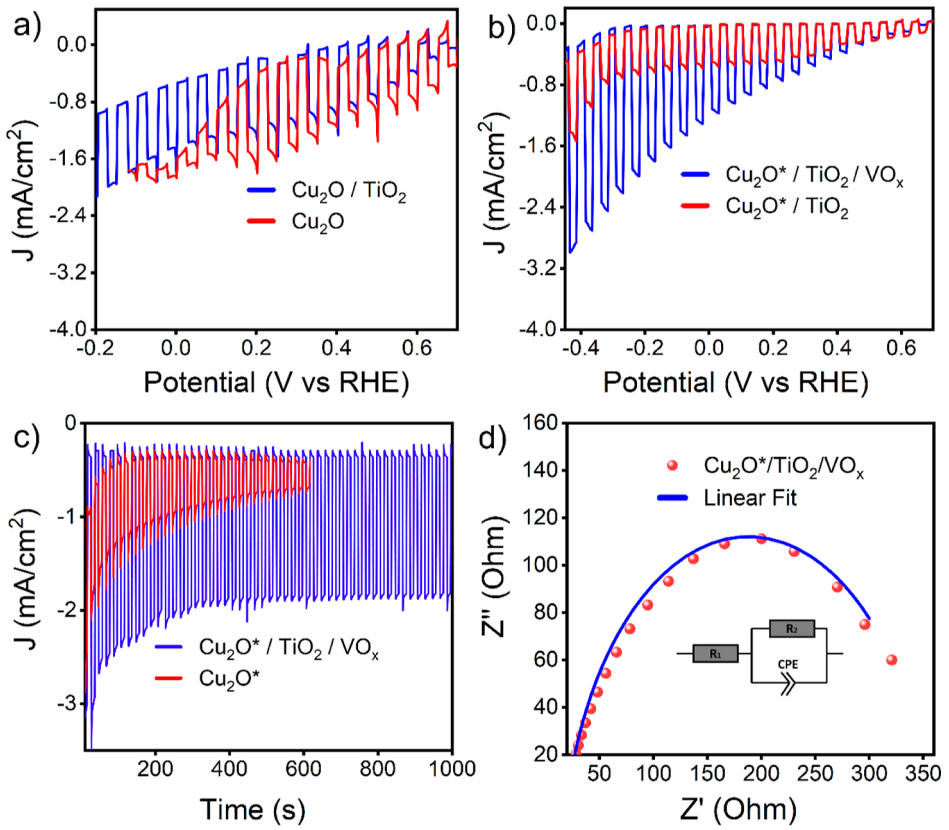

Figure 6. Plots of photocurrent vs applied potential for (a) Cu_2O and Cu_2O/TiO_2 and (b) Cu_2O^*/TiO_2 and $Cu_2O^*/TiO_2/VO_x$ (700 ALD cycles) photocathodes. (c) Chronoamperometry measurement (stability test) for Cu_2O^* and $Cu_2O^*/TiO_2/VO_x$ (700 ALD cycles) under chopped light at a bias voltage of −0.2 V (vs RHE) and (d) Nyquist plot for the $Cu_2O^*/TiO_2/VO_x$ (700 ALD cycles) photoelectrode.

cocatalyst are deposited on Cu_2O nanowires (Figure 5d). This outcome confirms that the addition of the electrodeposited Cu_2O between Cu_2O and the TiO_2/VO_x layers helps to reduce the photocorrosion and better protect the Cu_2O photoelectrode. In addition, diffuse reflectance measurements were carried out to estimate the band gap energy of the as-prepared photoelectrode (Figure S8a,b, Supporting Information). It is evident a very low reflectance signal for $Cu_2O^*/TiO_2/VO_x$, as expected, compared to the bare Cu_2O sample. By plotting the Kubelka−Munk function against photon energy $(\alpha h\nu)^n$ (where α is the absorption coefficient, $n = 2$ for the direct band gap semiconductor, and $h\nu$ is the photon energy), the band gap energy was estimated via extrapolation; an approximate energy gap of 2.2−2.4 eV is observed (Figure S8b), in agreement with the values reported in the literature.[6,8,9,16,17] The band gap of Cu_2O is not significantly altered by the protective layer (TiO_2) and the cocatalyst VO_x, as expected.

Mott−Schottky (M−S) plots are mostly used for determining the carrier density (N_A) and flat band potential of semiconductors. The M−S equation works for planar electrodes, the analysis for nonplanar photoelectrodes being more complicated.[9,11,12,25,26] However, various nanostructured photoelectrodes including Cu_2O are analyzed using the M−S plot.[17,23] In this work, to compare our results with previous investigations, we performed M−S analysis (Figure S8c,d). The slope of the C^{-2} versus applied potential shows negative slopes, as expected for p-type Cu_2O (Figure S8c,d). The total capacitance was calculated using eq S1 in the Supporting Information. In our case, the Helmholtz capacitor is not neglected because its value is much less than the space charge capacitance. For both samples, the flat band potential was obtained by extrapolating the linear part of $1/C_{sc}^2$ to $1/C_H^2$, which is 0.62 V versus RHE (according to eq S2, and Figure S8c in the Supporting Information).[8] Upon introducing the TiO_2 layer and the VO_x cocatalyst, the flat-band potential is found to be about 0.58 V versus RHE (Figure S8d in the Supporting Information). As expected, the presence of the TiO_2 layer and the cocatalyst alters the equilibrium of the Fermi level, resulting in a negative shift of the flat band potential from 0.62 to 0.58 V versus RHE.[23,27] The slope of the linear part of the M−S curve (Figure S8c in the Supporting Information) was used to calculate the carrier concentration (N_A), which results in 2.27×10^{18} cm^{-3} for the Cu_2O^* photoelectrode and 2.37×10^{18} cm^{-3} for $Cu_2O^*/TiO_2/VO_x$. In addition, to reveal the effect of VO_x cocatalyst amount on the photoelectrode, other two photoelectrodes ($Cu_2O^*/TiO_2/VO_x$), one with 500 ALD cycles and the other with 1000 ALD cycles, of the VO_x cocatalyst were produced and compared (Figure S9, results are discussed in the Supporting Information). On the basis of the obtained results, we decided that a 700 ALD cycle could be a good compromise to gain a good photostability and photocurrent; then, we continued to use the $Cu_2O^*/TiO_2/VO_x$ in further characterization.

In Figure 6a−d, the cathodic current density as a function of the applied potential under dark and light illumination conditions is provided. For all the photoelectrodes, when the bias voltage increases, a clear improvement in the photocurrent is observed. For bare Cu_2O nanowires and Cu_2O/TiO_2 (Figure 6a), a general increase in the dark current as a function of the potential was observed, suggesting a poor

https://doi.org/10.1021/acsaem.2c03122
ACS Appl. Energy Mater. 2023, 6, 832−840

stability of photoelectrodes. Also, for bare Cu_2O, the current under dark and light conditions becomes identical beyond 0.05 V versus RHE, while for the Cu_2O/TiO_2 sample, it is evident that the presence of the TiO_2 protective layer benefits the electrode to maintain its stability under similar conditions (Figure 6a). The photocurrent density of Cu_2O^*/TiO_2 (Figure 6b) at −0.3 V versus RHE is −0.8 mA/cm^2 under light and −0.23 mA/cm^2 under dark conditions, while the photocurrent densities of Cu_2O^*/TiO_2 with 700 cycles of the VO_x cocatalyst at −0.3 V versus RHE are −2.5 mA/cm^2 under light and −0.12 mA/cm^2 under dark conditions. Compared to Cu_2O^*/TiO_2, the performance of the photocathode with the VO_x cocatalyst is improved by more than threefold at −0.3 V versus RHE. The PEC performance for Cu_2O^*/TiO_2 and $Cu_2O^*/TiO_2/VO_x$ (Figure 6b) displays stable and improved performance, suggesting that the electrodeposited Cu_2O layer helps to minimize the shunt created between TiO_2 and Cu metal junction. In addition, the dark current in $Cu_2O^*/TiO_2/VO_x$ significantly diminished compared to Cu_2O/TiO_2 and bare Cu_2O, suggesting that the additional TiO_2 layer and VO_x cocatalyst suppressed self-corrosion by preventing the contact of Cu_2O with the electrolyte. Chronoamperometry measurements were carried out to study the stability of the photoelectrodes under chopped light illumination (Figures 6c and S10 in the Supporting Information). The bare Cu_2O photocathode (Figure S10) produces a stable photocurrent density of −0.2 mA/cm^2 just for a few minutes, and then, more than 50% photocurrent decays with time. This fast decrease in photocurrent density can be ascribed to the poor stability of the Cu_2O in contact with the electrolyte. In the case of the Cu_2O^* photoelectrode (Figure 6c), the oxidation of Cu_2O to CuO is still evident, as shown by the decay of the $J-V$ curve with time.

After the deposition of the thin layer of TiO_2 and 700 cycles of VO_x ($Cu_2O^*/TiO_2/VO_x$), much-improved stability of the photocurrent for extended illumination time with negligible loss of the photocurrent density is observed. This suggests that the introduction of the electrodeposited Cu_2O layer, the TiO_2 protective layer, and the cocatalyst VO_x layer unfolds a synergistic effect to improve the photostability of Cu_2O nanowires.

The charge transfer phenomena of the photoelectrode were explored using EIS measurement. Figure 6d shows the Nyquist plot for the $Cu_2O^*/TiO_2/VO_x$ (700 ALD cycles) photocathode in the frequency range from 100 kHz to 3 mHz obtained at a DC potential of 0.25 V versus RHE. The fitting parameters are listed in Table S1 in the Supporting Information. The inset of Figure 6d provides the equivalent circuit used for fitting the impedance data.[28,29] The resistance R_2 is associated with the charge transfer, which depends on the photocathode and the interface properties, while R_1 is related to solution resistance. CPE is a constant phase element associated with an imperfect capacitor.[30,31] The $Cu_2O^*/TiO_2/VO_x$ photoelectrode exhibits relatively lower charge transfer resistance (320 Ω) compared with the Cu_2O^*/TiO_2 photoelectrode (373 Ω, Figure S11 in the Supporting Information), suggesting its fast electron transfer at the solution−photoelectrode interface, leading to the better performance.

4. CONCLUSIONS

A photocathode based on Cu_2O nanowires was synthesized, and its PEC properties toward HER were investigated. Cu_2O has great potential as a photocathode for PEC water splitting, but its poor photostability is still limiting its broad application. Herein, we systematically studied a strategy to overcome this limitation by engineering the surface of the photocathode, eventually observing an improved photostability.

Then, the Cu_2O nanowires were successfully coated first with a layer of electrodeposited Cu_2O and then with a TiO_2 protective layer and a proper VO_x co-catalyst layer. The presence of these protective layers produced a significant increase in the photocurrent density (for $Cu_2O^*/TiO_2/VO_x$ at −0.3 V vs RHE, a current density of −2.46 mA/cm^2 under chopped light illuminations was recorded). In addition, the $Cu_2O^*/TiO_2/VO_x$ photocathode showed improved stability for extended illumination time, with negligible loss of the photocurrent density. These outcomes indicate that the presence of an electrodeposited Cu_2O helps reduce the recombination rate between the TiO_2 layer and Cu metal film. Moreover, the amorphous VO_x layer further protects Cu_2O from oxidation and acts as a co-catalyst. This study provides detailed insights into possible methods of engineering the Cu_2O photocathode to avoid or minimize the in situ oxidation during the PEC HER process.

■ ASSOCIATED CONTENT

Supporting Information

The Supporting Information is available free of charge at https://pubs.acs.org/doi/10.1021/acsaem.2c03122.

SEM image; EDS analysis; RBS and Raman; XRD pattern, EDS layered map; % reflectance and Kubelka−Munk plot; LSV; and chronoamperometry measurement (stability test) for Cu_2O (PDF)

■ AUTHOR INFORMATION

Corresponding Authors

Marta Maria Natile − *Institute of Condensed Matter Chemistry and Technologies for Energy (ICMATE), National Research Council (CNR) and Department of Chemical Sciences, University of Padova, Padova 35131, Italy;* orcid.org/0000-0001-5591-2670; Email: martamaria.natile@unipd.it, martamaria.natile@cnr.it

Alberto Vomiero − *Division of Materials Science, Department of Engineering Sciences and Mathematics, Luleå University of Technology, Luleå 971 87, Sweden; Department of Molecular Sciences and Nanosystems, Ca' Foscari University of Venice, Venezia Mestre 30172, Italy;* orcid.org/0000-0003-2935-1165; Email: alberto.vomiero@ltu.se, alberto.vomiero@unive.it

Authors

Getachew Solomon − *Division of Materials Science, Department of Engineering Sciences and Mathematics, Luleå University of Technology, Luleå 971 87, Sweden;* Present Address: Department of Chemical Engineering, KTH Royal Institute of Technology, Brinellvägen 8, 114 28 Stockholm, Sweden; orcid.org/0000-0001-6039-1865

Marco Lecca − *Institute of Condensed Matter Chemistry and Technologies for Energy (ICMATE), National Research Council (CNR) and Department of Chemical Sciences, University of Padova, Padova 35131, Italy;* Present Address: Department of Molecular Sciences and Nanosystems, Ca' Foscari University of Venice, via Torino 155, 30172 Venezia Mestre, Italy.

https://doi.org/10.1021/acsaem.2c03122
ACS Appl. Energy Mater. 2023, 6, 832−840

Matteo Bisetto − *Institute of Condensed Matter Chemistry and Technologies for Energy (ICMATE), National Research Council (CNR) and Department of Chemical Sciences, University of Padova, Padova 35131, Italy;* Present Address: Department of Chemical and Pharmaceutical Sciences, University of Trieste, via L. Giorgieri 1, 34127 Trieste, Italy.

Mojtaba Gilzad Kohan − *Division of Materials Science, Department of Engineering Sciences and Mathematics, Luleå University of Technology, Luleå 971 87, Sweden;* orcid.org/0000-0002-3956-444X

Isabella Concina − *Division of Materials Science, Department of Engineering Sciences and Mathematics, Luleå University of Technology, Luleå 971 87, Sweden;* orcid.org/0000-0003-1785-7177

Complete contact information is available at: https://pubs.acs.org/10.1021/acsaem.2c03122

Notes

The authors declare no competing financial interest.

■ ACKNOWLEDGMENTS

We acknowledge the financial support from the Kempe Foundation, the Knut & Alice Wallenberg Foundation, the Swedish Foundations consolidator fellowship, Luleå University of Technology laboratory fund program, and ICMATE-CNR project "Accordo di programma MiTE-ENEA (B93C22000630006)". M.L. and M.B. acknowledge the Erasmus+ for Studies program of the University of Padova and of the Luleå University of Technology.

■ REFERENCES

(1) Mazzaro, R.; Boscolo Bibi, S.; Natali, M.; Bergamini, G.; Morandi, V.; Ceroni, P.; Vomiero, A. Hematite Nanostructures: An Old Material for a New Story. Simultaneous Photoelectrochemical Oxidation of Benzylamine and Hydrogen Production through Ti Doping. *Nano Energy* **2019**, *61*, 36−46.

(2) Akilimali, R.; Selopal, G. S.; Mohammadnezhad, M.; Ka, I.; Wang, Z. M.; Lopinski, G. P.; Zhao, H.; Rosei, F. Structural Effect of Low-Dimensional Carbon Nanostructures on Long-Term Stability of Dye Sensitized Solar Cells. *Chem. Eng. J.* **2022**, *435*, 135037.

(3) Wang, X.; Zhang, Y.; Li, J.; Liu, G.; Gao, M.; Ren, S.; Liu, B.; Zhang, L.; Han, G.; Yu, J.; Zhao, H.; Rosei, F. Platinum Cluster/Carbon Quantum Dots Derived Graphene Heterostructured Carbon Nanofibers for Efficient and Durable Solar-Driven Electrochemical Hydrogen Evolution. *Small Methods* **2022**, *6*, 2101470.

(4) Solomon, G.; Kohan, M. G.; Landström, A.; Vomiero, A.; Concina, I. Semiconducting Metal Oxides Empowered by Graphene and Its Derivatives: Progresses and Critical Perspective on Selected Functional Applications. *J. Appl. Phys.* **2020**, *128*, 180905.

(5) Concina, I.; Ibupoto, Z. H.; Vomiero, A. Semiconducting Metal Oxide Nanostructures for Water Splitting and Photovoltaics. *Adv. Energy Mater.* **2017**, *7*, 1700706.

(6) Long, Z.; Tong, X.; Liu, C.; Channa, A. I.; Wang, R.; Li, X.; Lin, F.; Vomiero, A.; Wang, Z. M. Near-Infrared, Eco-Friendly ZnAgInSe Quantum Dots-Sensitized Graphene Oxide-TiO2 Hybrid Photoanode for High Performance Photoelectrochemical Hydrogen Generation. *Chem. Eng. J.* **2021**, *426*, 131298.

(7) Liccardo, L.; Lushaj, E.; Dal Compare, L. D.; Moretti, E.; Vomiero, A. Nanoscale ZnO/α-Fe_2O_3 Heterostructures: Toward Efficient and Low-Cost Photoanodes for Water Splitting. *Small Sci.* **2022**, *2*, 2100104.

(8) Wick, R.; Tilley, S. D. Photovoltaic and Photoelectrochemical Solar Energy Conversion with Cu2O. *J. Phys. Chem. C* **2015**, *119*, 26243−26257.

(9) Luo, J.; Steier, L.; Son, M. K.; Schreier, M.; Mayer, M. T.; Grätzel, M. Cu_2O Nanowire Photocathodes for Efficient and Durable Solar Water Splitting. *Nano Lett.* **2016**, *16*, 1848−1857.

(10) Salehmin, M. N. I.; Jeffery Minggu, L.; Mark-Lee, W. F.; Mohamed, M. A.; Arifin, K.; Jumali, M. H. H.; Kassim, M. B. Highly Photoactive Cu_2O Nanowire Film Prepared with Modified Scalable Synthesis Method for Enhanced Photoelectrochemical Performance. *Sol. Energy Mater. Sol. Cells* **2018**, *182*, 237−245.

(11) Wang, T.; Wei, Y.; Chang, X.; Li, C.; Li, A.; Liu, S.; Zhang, J.; Gong, J. Homogeneous Cu_2O P-n Junction Photocathodes for Solar Water Splitting. *Appl. Catal., B* **2018**, *226*, 31−37.

(12) Choi, J.; Song, J. T.; Jang, H. S.; Choi, M.-J.; Sim, D. M.; Yim, S.; Lim, H.; Jung, Y. S.; Oh, J. Interfacial Band-Edge Engineered TiO2 Protection Layer on Cu2O Photocathodes for Efficient Water Reduction Reaction. *Electron. Mater. Lett.* **2017**, *13*, 57−65.

(13) Paracchino, A.; Mathews, N.; Hisatomi, T.; Stefik, M.; Tilley, S. D.; Grätzel, M. Ultrathin Films on Copper(I) Oxide Water Splitting Photocathodes: A Study on Performance and Stability. *Energy Environ. Sci.* **2012**, *5*, 8673−8681.

(14) Tilley, S. D.; Schreier, M.; Azevedo, J.; Stefik, M.; Graetzel, M. Ruthenium Oxide Hydrogen Evolution Catalysis on Composite Cuprous Oxide Water-Splitting Photocathodes. *Adv. Funct. Mater.* **2014**, *24*, 303−311.

(15) Solomon, G.; Kohan, M. G.; Vagin, M.; Rigoni, F.; Mazzaro, R.; Natile, M. M.; You, S.; Morandi, V.; Concina, I.; Vomiero, A. Decorating Vertically Aligned MoS2 Nanoflakes with Silver Nanoparticles for Inducing a Bifunctional Electrocatalyst towards Oxygen Evolution and Oxygen Reduction Reaction. *Nano Energy* **2021**, *81*, 105664.

(16) Gilzad Kohan, M. G.; Solomon, G.; You, S.; Yusupov, K.; Concina, I.; Vomiero, A. Vertically Aligned Co_3O_4 Nanorods as a Platform for Inverted All-Oxide Heterojunctions. *Nano Sel.* **2021**, *2*, 967−978.

(17) Dizajghorbani Aghdam, H.; Moemen Bellah, S.; Malekfar, R. Surface-Enhanced Raman Scattering Studies of Cu/Cu_2O Core-Shell NPs Obtained by Laser Ablation. *Spectrochim. Acta, Part A* **2019**, *223*, 117379.

(18) Lu, C.; Li, Z.; Ren, L.; Su, N.; Lu, D.; Liu, Z. In Situ Oxidation of Cu2O Crystal for Electrochemical Detection of Glucose. *Sensors* **2019**, *19*, 2926.

(19) Zhong, J. H.; Li, G. R.; Wang, Z. L.; Ou, Y. N.; Tong, Y. X. Facile Electrochemical Synthesis of Hexagonal Cu2O Nanotube Arrays and Their Application. *Inorg. Chem.* **2010**, *50*, 757−763.

(20) Dhananjaya, M.; Prakash, N. G.; Sandhya, G. L.; Narayana, A. L.; Hussain, O. M. Microstructure and Supercapacitor Properties of V_2O_5 Thin Film Prepared by Thermal Evaporation Method 1; *Mater. Sci. Eng.* **2017**.

(21) Shvets, P.; Maksimova, K.; Goikhman, A. Correlation between Raman Spectra and Oxygen Content in Amorphous Vanadium Oxides. *Phys. B* **2021**, *613*, 412995.

(22) Le Van, K.; Groult, H.; Mantoux, A.; Perrigaud, L.; Lantelme, F.; Lindström, R.; Badour-Hadjean, R.; Zanna, S.; Lincot, D. Amorphous Vanadium Oxide Films Synthesised by ALCVD for Lithium Rechargeable Batteries. *J. Power Sources* **2006**, *160*, 592−601.

(23) Lee, K.; Lee, S.; Cho, H.; Jeong, S.; Kim, W. D.; Lee, S.; Lee, D. C. Cu^+-Incorporated TiO_2 Overlayer on Cu_2O Nanowire Photocathodes for Enhanced Photoelectrochemical Conversion of CO_2 to Methanol. *J. Energy Chem.* **2018**, *27*, 264−270.

(24) Shoesmith, D. W.; Sunder, S.; Bailey, M. G.; Wallace, G. J.; Stanchell, F. W. Anodic Oxidation of Copper in Alkaline Solutions: Part IV. Nature of the Passivating Film. *J. Electroanal. Chem. Interfacial Electrochem.* **1983**, *143*, 153−165.

(25) Szaniawska, E.; Rutkowska, I. A.; Frik, M.; Wadas, A.; Seta, E.; Krogul-Sobczak, A.; Rajeshwar, K.; Kulesza, P. J. Reduction of Carbon Dioxide at Copper(I) Oxide Photocathode Activated and Stabilized by over-Coating with Oligoaniline. *Electrochim. Acta* **2018**, *265*, 400−410.

(26) Sivula, K. Mott-Schottky Analysis of Photoelectrodes: Sanity Checks Are Needed. *ACS Energy Lett.* **2021**, *6*, 2549−2551.

(27) Yang, Y.; Xu, D.; Wu, Q.; Diao, P. Cu_2O/CuO Bilayered Composite as a High-Efficiency Photocathode for Photoelectrochemical Hydrogen Evolution Reaction. *Sci. Rep.* **2016**, *6*, 35158.
(28) Solomon, G.; Landström, A.; Rotta Loria, S.; Bolli, E.; Mezzetti, A.; Facibeni, A.; Cattarin, S.; Mezzi, A.; Protti, S.; Kaciulis, S.; Zavelani-Rossi, M.; Concina, I. Tunable Physics through Coordination Chemistry: Formation on Oxide Surface of Ti and Al Chelates with 3-Hydroxyflavone Capable of Electron Injection and Light Emission. *Dalton Trans.* **2022**, *51*, 18489−18501.
(29) Solomon, G.; Kohan, M. G.; Mazzaro, R.; Jugovac, M.; Moras, P.; Morandi, V.; Concina, I.; Vomiero, A. MoS_2 Nanosheets Uniformly Anchored on $NiMoO_4$ Nanorods, a Highly Active Hierarchical Nanostructure Catalyst for Oxygen Evolution Reaction and Pseudo-Capacitors. *Adv. Sustainable Syst.* **2022**, 2200410.
(30) Shifa, T. A.; Yusupov, K.; Solomon, G.; Gradone, A.; Mazzaro, R.; Cattaruzza, E.; Vomiero, A. In Situ-Generated Oxide in Sn-Doped Nickel Phosphide Enables Ultrafast Oxygen Evolution. *ACS Catal.* **2021**, *11*, 4520−4529.
(31) Solomon, G.; Landström, A.; Mazzaro, R.; Jugovac, M.; Moras, P.; Cattaruzza, E.; Morandi, V.; Concina, I.; Vomiero, A. $NiMoO_4$@Co_3O_4 Core−Shell Nanorods: In Situ Catalyst Reconstruction toward High Efficiency Oxygen Evolution Reaction. *Adv. Energy Mater.* **2021**, *11*, 2101324.

https://doi.org/10.1021/acsaem.2c03122
ACS Appl. Energy Mater. 2023, 6, 832−840